Journal of Hazardous Materials 171 (2009) 102–110

Contents lists available at ScienceDirect

Journal of Hazardous Materials

journal homepage: www.elsevier.com/locate/jhazmat

Collection of SiO_2, Al_2O_3 and Fe_2O_3 particles using a gas-solid fluidized bed filter

Kuang-Yu Liu[a], Jui-Yeh Rau[b], Ming-Yen Wey[b,*]

[a] Department of Safety, Health and Environmental Engineering, National United University, Miao-Li 360, Taiwan, ROC
[b] Department of Environmental Engineering, National Chung Hsing University, Taichung 402, Taiwan, ROC

ARTICLE INFO

Article history:
Received 5 November 2008
Received in revised form 26 May 2009
Accepted 26 May 2009
Available online 6 June 2009

Keywords:
Fluidized bed filter
Particle filtration
Collection mechanism
Particle size distribution

ABSTRACT

The filtration of SiO_2, Al_2O_3 and Fe_2O_3 particles with average sizes of 4 and 40 μm using a fluidized bed filter at 40 and 300 °C was studied. The collection mechanisms, interparticle forces and bounce-off effect between filtered particles and collectors were analyzed to determine their effect on particle filtration. Experimental results showed that the collection efficiency of 4 μm SiO_2 and Al_2O_3 particles exceeded that of 40 μm particles. Contrarily, the 40 μm Fe_2O_3 particles were collected more efficiently than the 4 μm particles, because of the differences between the microstructures of SiO_2, Al_2O_3, and Fe_2O_3 particles. The interaction between the particles affected the removal of mixed SiO_2, Al_2O_3 and Fe_2O_3. The particle size distribution (PSD) of the particles in the exit was governed by the operating temperature, the original size of the filtered particles, the interparticle force and the hardness of the particles and the collectors. The smallest particles were not those most easily elutriated from the fluidized bed filter because they agglomerated with each other or with large particles. The van der Waal's force dominated the forces between 4 and 40 μm particles. The main collection mechanism for 4 and 40 μm particles was direct interception. The effect of impaction increased with particle size above 40 μm. The strong impaction and bounce-off effect reduced the collection efficiency of 40 μm SiO_2 and Al_2O_3 particles. However, the strong interparticle force between Fe_2O_3 particles and collectors contributed to the high collection efficiency of the Fe_2O_3 particles.

1. Introduction

Granular beds are widely adopted for particle filtration in a gas stream. New (since the 1970s) energy production systems such as Pressurized Fluidized Bed Combustion and the Integrated Gasification Combined Cycle have stimulated study of particulate removal at high temperatures. The particulates and other contaminants must be removed to protect the gas turbine. Fluidized bed filters have been adopted to filter particles. Knettig and Beeckmans [1] studied the capture of aerosols of sizes 0.8–2.9 μm in a fixed and fluidized bed filter; capture efficiency increased with bed height. Doganoglu et al. [2] focused on the effects of the various parameters on particle filtration, including superficial gas velocity, static bed height, the species of collector particle and the distributor. Tardos et al. [3] employed a numerical solution to the diffusion equation to calculate the single sphere collection efficiency for small particles in a fluidized bed filter. Peters et al. [4], Ushiki and Tien [5,6] proposed models to calculate the collection efficiency in fluidized bed filters.

When a fluidized bed filter is used to filter particles, both mechanisms – aerosol capture by filter grains and the elutriation of particles – should be considered. The mechanisms for collecting particles include interception, inertial impaction, diffusion, gravitational settling and electrostatic attraction; the efficiency of each mechanism is dominated by the characteristics of the particles, the collecting media and the treated gas, such as flow velocity and temperature. The interparticle forces, such as the van der Waal's, the liquid-bridging and the electrostatic force, determine the elutriation, which may also be affected by the species of particles [7], temperature [8], gas flow rate [9] and humidity [10]. These works addressed only the effect of various parameters on elutriation. Additionally, Ghadiri et al. [11] considered the re-entrainment of the particles from the bed material and noted that the removal efficiency declined extensively when bounce off occurred. However, the filtration of particles in a fluidized bed involves a balance among the collection, accumulation and elutriation of fines. The influence of the interparticle forces and other parameters on particle filtration in a fluidized bed filter was seldom studied

Hot gas filtration with a fluidized bed filter is of interest because a fluidized bed removes not only particles but also the organics and acid gases in flue gas [12–15]; it can also be used as a heat exchanger. In this study, SiO_2, Al_2O_3 and Fe_2O_3 particles were filtered using fluidized beds. The collection efficiency and particle size distribution in the exhaust gas were measured. Additionally, the effects of interparticle forces, collection mechanisms and bounce off on particle filtration were studied.

* Corresponding author. Tel.: +886 4 22852455; fax: +886 4 22862587.
E-mail address: mywey@dragon.nchu.edu.tw (M.-Y. Wey).

0304-3894/$ – see front matter © 2009 Elsevier B.V. All rights reserved.
doi:10.1016/j.jhazmat.2009.05.129

Nomenclature

a	surface separation between two particles
A	Hamaker constant
C_c	Cunningham correction factor
D	bed diameter
d_c	collector (sphere) diameter
d_p	particle diameter
D_p	particle diffusion coefficient
E_D, E_G, E_I, E_R	single sphere collection efficiency of diffusion, gravity impaction and interception separately
E_d	breakdown potential of air
$\|F\|_{max}$	maximum particle electrostatic force
F_{vw}	van der waals force
g	acceleration of gravity
G_a	Galileo number
k	Boltzman constant
P_e	Pelect number
PM_{10}, $PM_{2,5}$, $PM_{1,0}$	particulate matters less than 10, 2.5 and 1.0 μm
PSD	particle size distribution
$\|q\|_{max}$	maximum particle electrostatic charge
R	sphere radius
R_{ef}	Reynolds number of collector
RMS	root mean square for hemisphere asperities
S_t	Stokes number
T	absolute gas temperature
U_f	operating gas velocity
U_{mf}	minimum fluidization velocity

Greek letters

ε_0	relative permittivity of free space
$\bar{\varepsilon}$	bed porosity
γ	adhesion probability
λ	mean free path of gas molecules
μ	gas dynamic viscosity
ρ_b	fluidized bed density
ρ_p	particle density

2. Collection mechanisms and interparticle forces

2.1. Collection mechanisms and bounce-off effect

The collection mechanisms that are associated with filtration in fluidized bed filter are inertial impaction, interception, diffusion, gravity and electrical effect. Inertial impaction and gravity are valid for relatively large particles of tens of microns. The effect of diffusion increased slowly as the particle size fell into the submicron range and dominated in the case of the nanoparticles. Interception is important for small particles in the order of submicrons to several microns. In some works, these collection mechanisms in a granular bed have been studied and some reciprocal equations for the various collection mechanisms were introduced [16–18]. In this study, similar mechanisms were employed to obtain experimental data concerning particle collection in fluidized bed filters.

When aerosol particles in a gas came into contact with a granule in the filter, the particles either rebounded or were retained by the bed material [19]. The bounce-off effect occurred when inertia impaction dominated. Generally, inertial impaction became significant at high gas velocity or for large particles – that is at a large Stokes number (S_t). Tien [20] introduced the coefficient of adhesion probability, γ, to explain this effect. γ is given by

$$\gamma = 0.00318 {S_t}^{-1.248} \quad (1)$$

For dry particles, the bounce-off effect should be considered when $S_t > 0.01$.

2.2. Interparticle forces

Interparticle forces occur for various reasons. In a fluidized bed filter, the significant ones are the van der Waal's force, capillary force, gravity and electrostatic force. The capillary force is related to the relative humidity. A point of relative humidity exists at which the capillary force begins to appear and below which it is absent [21]. Coelho and Harnby [22] found that the critical relative humidity was in the range of 70–99%, based on thermodynamic equilibrium. In this study, the relative humidity of the inlet gas was 20–25%, which is far below the suggested critical value. Hence, the capillary force was ignored.

The van der Waal's force is the most common interparticle force because it always exists and dominates the bulk behaviors of fine particles. Some theories have been proposed for calculating the van der Waal's force. They include the Hamaker [23], JKR [24], DMT [25], and Rumpf [26]–Rabinovich model [27]. The application of the JKR and DMT models is difficult because of the complexity of the estimation of the surface energy [21]. Rumpf–Rabinovich modified the Hamaker model to consider the effect of asperity on van der Waal's force. The Hamaker and Rumpf–Rabinovich (R–R) models are:

$$F_{vw} = \frac{AR}{12a^2} \quad \text{Hamaker} \quad (2)$$

$$F_{vw} = \frac{AR}{12a^2}\left(\frac{1}{1 + R/1.48\text{RMS}} + \frac{1}{(1 + 1.48\text{RMS}/a)^2}\right) \quad R-R \quad (3)$$

where A is Hamaker constant, R is the sphere radius, a is the surface separation and RMS is the root mean square for hemisphere asperities.

In a fluidized bed filter, particles are charged by colliding with each other or with the wall of the fluidized bed filter. A microscopic discussion on the electrostatic force for a single particle is impractical because the electrical charge and the polarity of charges of the various particles differ. Revel et al. [28] proposed a model to calculate the maximum particle electrostatic charge and electrostatic force.

$$|q|_{max} = \frac{2\pi\varepsilon_0}{3}\frac{d_p^3 E_d}{(1-\bar{\varepsilon})D} \quad (4)$$

$$|F|_{max} = \frac{2\pi\varepsilon_0}{3}\frac{d_p^3 E_d^2}{(1-\bar{\varepsilon})D}\frac{\rho_p}{\rho_b} \quad (5)$$

where ε_0 is the relative permittivity or dielectric constant of free space, E_d is the breakdown potential of air, $\bar{\varepsilon}$ is bed porosity, D is bed diameter and ρ_b is fluidized bed density ($\rho_b = (1-\bar{\varepsilon})\rho_p$). The Revel model excludes the electrostatic force from the external electrical field, and only takes the weak Coulombic force into consideration.

3. Experimental

3.1. Materials and equipment

The experimental system is modified from that based on the one used in the authors' earlier work and the details of the apparatus are discussed below [29]. Fig. 1 schematically depicts it. The powder feeder was mounted on top of the pre-heater. The filtered particles were lifted into the powder feeder and then fell into the inlet gas by gravity. Silica sand of size 701–840 μm and density 2650 kg m^{-3} was the collecting media. The compositions of the silica sand were SiO_2 (>98.5 wt%), Al_2O_3 (<0.15 wt%) and Fe_2O_3

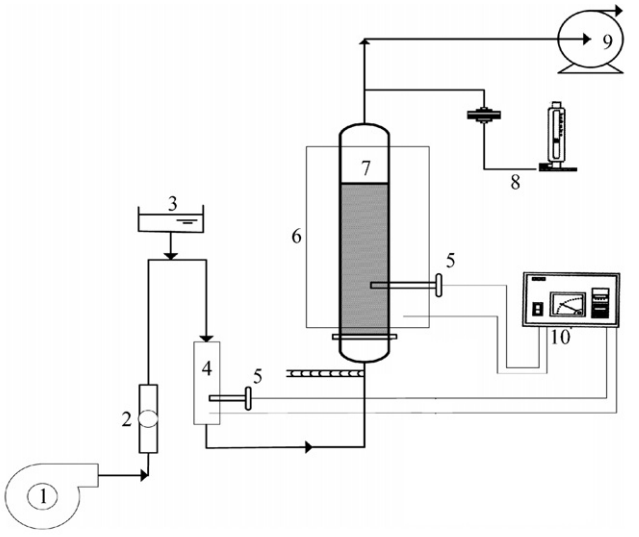

Fig. 1. Fluidized bed filter.

(<0.015 wt%). The distributor was a perforated stainless steel plate with holes of 0.7 mm in diameter. In the authors' previous studies, a fluidized bed filter was used to collect the fly ash from a coal-fired boiler. SiO_2, Al_2O_3 and Fe_2O_3 were major components of the fly ash [30]. Therefore, SiO_2, Al_2O_3 and Fe_2O_3 particles were used herein to study the influence of the various parameters on the particle filtration. Commercial SiO_2 Al_2O_3 and Fe_2O_3 particles were purchased for the testing. The mean diameter of these commercial particles was selected to be about 4 and 40 μm because particles of these two sizes were abundant in the fly ash. The PSD of the particles in the exhaust gas was measured with a cascade impactor (Anderson Co. Ltd., model: AS 500, analyze range: 0.36–31 μm).

3.2. Experimental procedure

3.2.1. Elutriation test of bed material

The bed materials can always be elutriated from the fluidized bed filter. The elutriated bed material represents the background mass and must be subtracted from the total mass of the collected particles in the filtration. Accordingly, the elutriated concentration and PSD of the bed material are tested. Before the test, the inner column of the fluidized bed filter and the ducts were cleaned to prevent errors during the experiment. The silica sand was placed into the bed to a static height of 21 cm. The pre-heater and the fluidized bed filter were heated to 40 or 300 °C, respectively. Then, air was supplied until a stable temperature was maintained. The minimum fluidization velocity (U_{mf}) was determined using a U-tube manometer. The operating gas velocity (U_f) was maintained at 0.50 m s^{-1}, which corresponds to U_f/U_{mf} = 1.32 and 1.34 at 40 and 300 °C, respectively. A sample of the elutriated concentration was extracted hourly at the beginning of the 6 h period before a steady concentration was reached. Then, the PSD of the elutriated bed material was measured. The sampling time was 3 h to ensure that an adequate amount of particles were present on the filter. Glass fiber filters were used as a collection medium in the tests. The elutriated concentration and PSD of the bed material were subtracted from that of the output particles to yield the exact outlet concentrations. Most of the elutriated concentrations were lower than 5% and the elutriated PSD was lower than 10% of the outlet concentration. After the elutriation test, the filtration test was performed without replacing the silica sand.

3.2.2. Filtration of SiO_2, Al_2O_3 and Fe_2O_3 particles

Following the elutriation test, the weighed particles were put into the powder feeder and injected into the inlet gas. A constant input rate was maintained throughout the test. The driving speed of the particle feeder was regulated to a constant input rate of 403.3 ± 12.0 mg min^{-1} for SiO_2 and 620.8 ± 21.3 mg min^{-1} for Al_2O_3 and 702 ± 23.3 mg min^{-1} for Fe_2O_3, corresponding to concentrations of 712 ± 21, 1096 ± 38 and 1240 ± 41 mg min^{-1}, respectively. The input rates of Al_2O_3 and Fe_2O_3 exceeded that of SiO_2 because Al_2O_3 and Fe_2O_3 were denser and had a lower packing voidage. After the experiment, the distributor plate and ducts were removed and the particles on it were weighed; their masses were subtracted from the input mass to calculate the input concentration of particles. The sampling at the outlet of the fluidized bed filter was begun simultaneously with isokinetic sampling when the particles were injected. At an operating temperature of 40 °C, the period for each sampling was three min and renewing the filter took two min. At 300 °C, the sampling time was also three min but renewing the filter took four min. At high temperature, a cooling system was installed after the filter holder in the sampling train to reduce the temperature of the gas to room temperature. Therefore, renewing the filter took more time at 300 °C so the samples were fewer than at 40 °C. These tasks were repeated for a total time of 35 min and sampling was immediately performed to determine PSD. The sampling time was 12–15 min in PSD tests of SiO_2, Al_2O_3 and Fe_2O_3 particles until a total run time of 50 min was reached. The sampling time varied because the proper mass had to be collected on the filters of the cascade impactor. The sampling flow rate was calibrated and regulated for isokinetic sampling. Table 1 lists the experimental conditions.

3.2.3. Chemical compositions of variously sized particles

When SiO_2, Al_2O_3 and Fe_2O_3 particles were captured by the bed material, they were abraded generating fine powders. These fine powders adhered to the bed material or coagulated with each other. They were then elutriated from the bed. The chemical composition distribution of variously sized particles in the exhaust gas helped to explain the filtration behaviors. The particles collected at each stage of the cascade impactor were extracted by microwave digestion. The compositions of Al, Si and Fe in the samples were analyzed using an ionic couple plasma detector. The background concentration of the

Table 1
Experimental conditions.

Bed material	Silica sand		
Sand density	2650 kg m^{-3}	Sand size	701–840 μm
Bed size	Diameter: 15.5 cm	Height: 80 cm	
Static height	21 cm		
Bed temperature	40, 300 °C		
Gas velocity[a]	0.50 m sec^{-1}		
U_{mf}	0.38[b], 0.37[c]	U_f/U_{mf}	1.32[b], 1.34[c]
Input particle	SiO_2, Al_2O_3 and Fe_2O_3		
Average particle size	4, 40 μm		
Feed rate (mg/min^{-1})	SiO_2: 403 ± 12; Al_2O_3: 621 ± 21; Fe_2O_3: 702 ± 23		
Input concentration (mg/m^{-3})	SiO_2: 712 ± 21; Al_2O_3: 1097 ± 38; Fe_2O_3: 1240 ± 41		
Run time	50 min		
Relative humidity	20–25% (40 °C)		

[a] Gas velocity has been calibrated to 40 and 300 °C.
[b] The bed temperature is at 40 °C.
[c] The bed temperature is at 300 °C.

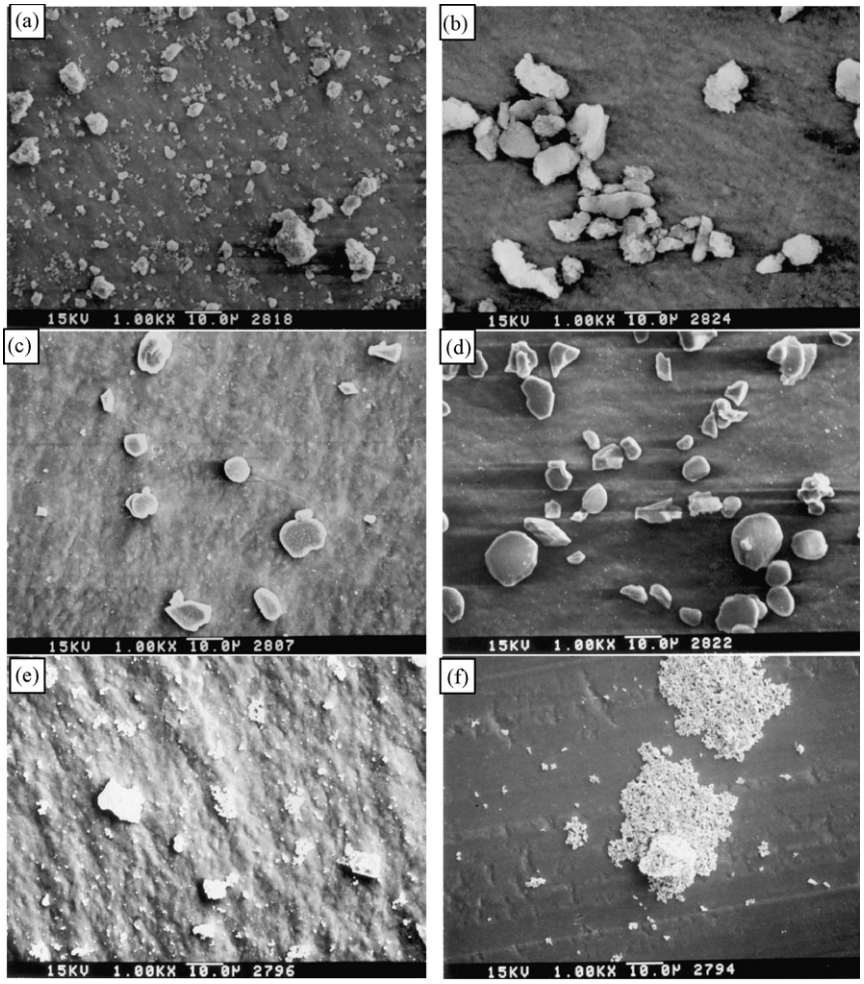

Fig. 2. Surface microstructure of SiO_2, Al_2O_3 and Fe_2O_3 particles by SEM (×1000).

filter was subtracted. The Al, Si and Fe were assumed to be Al_2O_3, SiO_2 and Fe_2O_3 since they were particles to be filtered.

4. Results and discussion

4.1. Surface microstructures of the original SiO_2, Al_2O_3 and Fe_2O_3 particles

Surface phenomena affect the interaction between particles when they come into contact. In this study, commercial SiO_2, Al_2O_3 and Fe_2O_3 particles of sizes 4 and 40 μm were used. The surface microstructure of these originally purchased particles, presented in Fig. 2, was examined by scanning electron microscopy. Fig. 2(a) depicts the structure of 4 μm SiO_2 particles. There were particles of different sizes, and some particles were even larger than 10 μm. The actual size of 40 μm SiO_2 particles seemed to be smaller than the stated size, as displayed in Fig. 2(b), but most were larger than the 4 μm particles. The SiO_2 particles exhibited were separate with irregular shapes. Fig. 2(c), (d) presents photographs of Al_2O_3 particles. The Al_2O_3 particles were almost round. They were separate as were the SiO_2 particles. The structure of Fe_2O_3 particles, shown

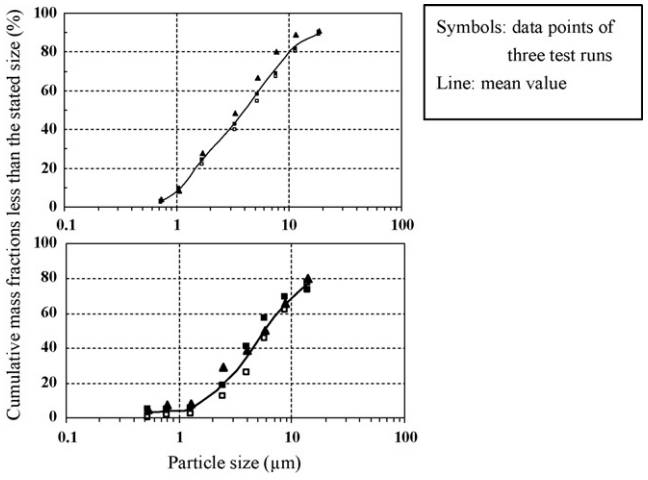

Fig. 3. Particle size distribution of the elutriated bed material at (a) 300; (b) 40 °C.

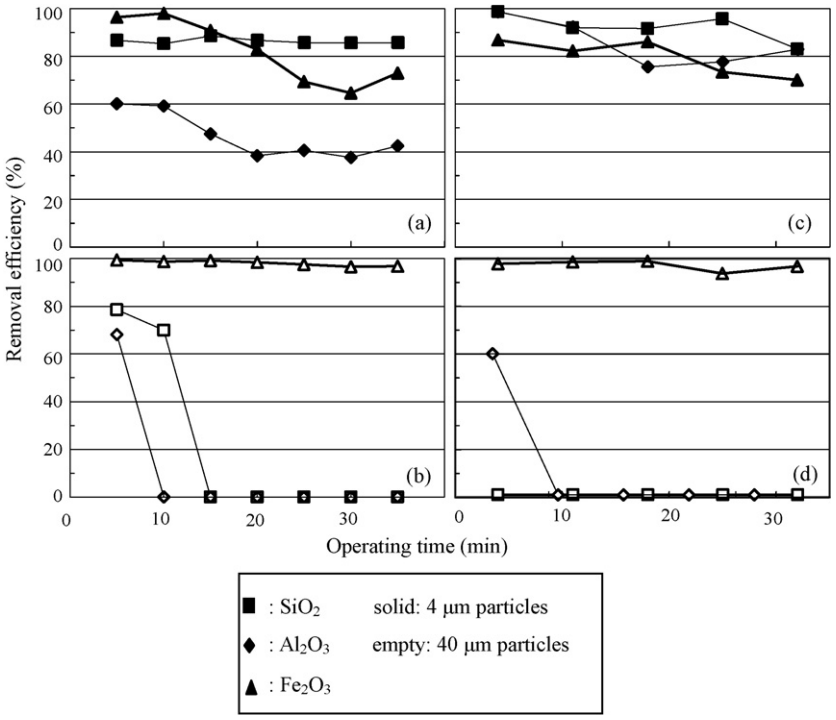

Fig. 4. Removal efficiency of individual SiO_2, Al_2O_3 and Fe_2O_3 particles. (a),(b) at 4; (c),(d) at 300 °C.

in Fig. 2(e), (f), differed from that of SiO_2 and Al_2O_3. The Fe_2O_3 particles were originally submicron particles. These small particles aggregated to form large particles of various sizes. The Fe_2O_3 particles aggregated to a large size because of their strong interparticle forces. These forces helped to remove Fe_2O_3 particles using a fluidized bed filter.

4.2. Particle size distribution of elutriated silica sand

Fig. 3 depicts the PSD of the elutriated bed material at 40 and 300 °C. Each experiment was performed three times to check the consistency of the results. At a temperature of 300 °C, PM_{10} of the elutriated silica sand was 80%, $PM_{2.5}$ was 35% and $PM_{1.0}$ was 9%, as shown in Fig. 3(a). Fig. 3(b) presents the PSD of the elutriated bed material at 40 °C. The fractions of PM_{10}, $PM_{2.5}$ and $PM_{1.0}$ were 70%, 20% and 4%. At 300 °C, more small particles were elutriated from the fluidized bed filter than at 40 °C. The particles were strongly abraded into small ones at high temperature.

4.3. Removal efficiency of the filtered particles

4.3.1. Filtration of separate SiO_2, Al_2O_3 and Fe_2O_3 particles

Fig. 4 plots the removal efficiencies of separate SiO_2, Al_2O_3 and Fe_2O_3 particles. The mass of elutriated bed material and that of the particles that remained on the distributor and duct were subtracted from the input data to determine the real removal efficiency of a fluidized bed filter. Fig. 4(a) plots the removal efficiency of 4 μm particles at 40 °C. The removal efficiency of the 4 μm SiO_2 particles was maintained at 85–89%. However, for the Al_2O_3 particles, it decreased from 60% to 40%. The removal efficiency of Fe_2O_3 particles decreased from 98% initially to a minimum of 65% over time. Fig. 4(b) plots the removal efficiencies of SiO_2, Al_2O_3 and Fe_2O_3 particles of 40 μm at 40 °C. The removal efficiencies of the SiO_2 and Al_2O_3 particles decayed sharply from about 80% and 70% to no efficiency at 10 or 15 min after the beginning of the test. However, the removal efficiency of the Fe_2O_3 particles was as high as 97–99% throughout the test. The efficiency of the 40 μm Fe_2O_3 particles exceeded that of the 4 μm Fe_2O_3 particles. The reason for the different removal efficiency of separate 4 μm and 40 μm SiO_2 and Al_2O_3 particles was attributed to the bounce-off effect. The strong bounce-off effect of the 40 μm particles lowered the removal efficiency, as discussed in Section 4.7.

Fig. 4(c), (d) presents the separate removal efficiencies of the 4 and 40 μm particles at 300 °C. The efficiencies of the 4 μm SiO_2 particles ranged from 83–99%. The removal efficiency of the Al_2O_3 particles fell from 99% to around 80% and that of Fe_2O_3 particles from 87% to 70%. Furthermore, the removal of the 4 μm particles at 300 °C was more efficient than at 40 °C. The removal efficiency of the 40 μm particles at 300 °C was similar to that at 40 °C. Neither SiO_2 nor Al_2O_3 particles could be removed efficiently at 300 °C. The removal efficiency of Fe_2O_3 particles was 94–99%, and overcame that of the 4 μm FeO_3 particles.

4.3.2. Filtration of mixed SiO_2, Al_2O_3 and Fe_2O_3 particles

When various particles were filtered using a fluidized bed filter, not only the properties of individual particles but also the interaction between particles affected the removal efficiency. Therefore, the filtration of the mixed SiO_2, Al_2O_3 and Fe_2O_3 particles was examined. The mixing mass ratio of these particles (5:3:2) was

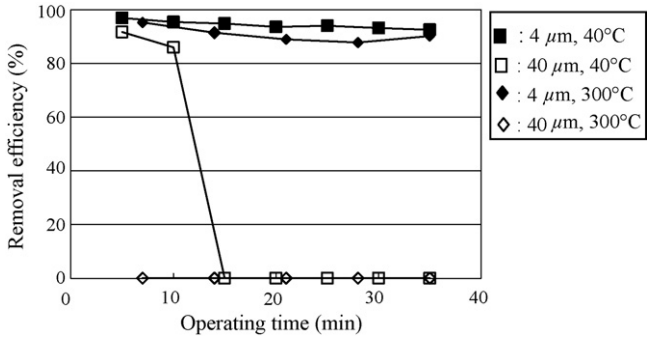

Fig. 5. Removal efficiency of mixed SiO_2, Al_2O_3 and Fe_2O_3 particles.

determined for the specific SiO_2, Al_2O_3 and Fe_2O_3 particle contents of the fly ash in the exhaust gas of a coal-fired power generation plant [30]. Fig. 5 depicts the collection efficiency of mixed particles. For the 40 μm mixed particles, the removal efficiency at 40 °C decreased sharply from 93% to zero, like the removal of separate SiO_2 and Al_2O_3 particles of 40 μm. The removal efficiency of the 40 μm mixed particles at 300 °C showed the same trend as that at 40 °C. The presence of 40 μm Fe_2O_3 particles did not influence the removal efficiency of mixed particles, even when its content was 20%. The bounce-off effect of the 40 μm SiO_2, and Al_2O_3 particles overcame the coagulation of the Fe_2O_3 particles. The removal efficiency of the 4 μm mixed particles was 87–95% at 300 °C and was 92–97% at 40 °C, which came close to the efficiency of the 4 μm separate SiO_2 particles. The removal efficiency of the mixed particles of 4 μm was not influenced by the bounce-off effect.

4.4. Size distributions of SiO_2, Al_2O_3 and Fe_2O_3 particles in exhaust gas

Fig. 6 displays the PSD of filtered SiO_2, Al_2O_3 and Fe_2O_3 particles in exhaust gas at 40 and 300 °C. The mass of the elutriated bed material was subtracted from the mass of particles collected on the filter. Fig. 6(a), (b) shows the PSD of SiO_2 particles of sizes 4 and 40 μm. The percentages of PM_{10}, $PM_{2.5}$ and $PM_{1.0}$ ($PM_{10}/PM_{2.5}/PM_{1.0}$) in 4 μm particles were 70%, 21% and 10% at 40 °C and 45%, 12% and 7% at 300 °C. For the 40 μm particles, $PM_{10}/PM_{2.5}/PM_{1.0}$ at 40 °C were 38%, 1.1% and 0.7% and the corresponding values at 300 °C were 32%, 1.5% and 0.5%. When the 40 μm particles were filtered, the PSD shifted to the large particles than that of 4 μm particles. Moreover, the amount of the particles larger than 10 μm at 300 °C was more than that at 40 °C. Fig. 6(c), (d) plots the PSD of the filtered 4 and 40 μm Al_2O_3 particles. $PM_{10}/PM_{2.5}/PM_{1.0}$ of the filtered 4 μm particles were 70%, 2% and 0.5% at 40 °C and 50%, 2% and 0.5% at 300 °C. The $PM_{10}/PM_{2.5}/PM_{1.0}$ values of the 40 μm particles were 18%, 2% and 0.5% at 40 °C and 10%, 0.3% and 0.2% at 300 °C. The Al_2O_3 particles were less abraded in the bed because Al_2O_3 was harder than the bed material of silica sand (Mohs' hardness of Al_2O_3 and silica sand was 9 and 7, respectively). Hence, the number of particles larger than 10 μm dominated when the 40 μm Al_2O_3 particles were filtered. Additionally, the number of large particles of the filtered 4 and 40 μm particles at 300 °C exceeded the number of small particles at 40 °C. Fig. 6(e), (f) plots the PSD values of the 4 and 40 μm Fe_2O_3 particles that were filtered. For the 4 μm particles, $PM_{10}/PM_{2.5}/PM_{1.0}$ were 13%, 3% and 2% at 40 °C and 40%, 10% and 3% at 300 °C. For the 40 μm particles, $PM_{10}/PM_{2.5}/PM_{1.0}$ were 75%, 38% and 28% at 40 °C and 71%, 27% and 19% at 300 °C. The PSD of the Fe_2O_3 particles differed from that of the SiO_2 and Al_2O_3 particles. When the 40 μm Fe_2O_3 particles were filtered, the Fe_2O_3 particles in the exhaust gas were mostly small (PM_{10} was as high as 71% and 75%). However, the PSD shifted toward the large particles when the 4 μm Fe_2O_3 particles were filtered. As aforementioned, the large Fe_2O_3 particles were aggregated from the small particles, and Fe_2O_3 was less hard than silica sand. Moreover, many 40 μm Fe_2O_3 particles were captured by silica sand since the removal efficiency was high. These large particles were easily abraded and cracked into small particles. Accordingly, numerous small particles were present at the exit of the fluidized bed filter.

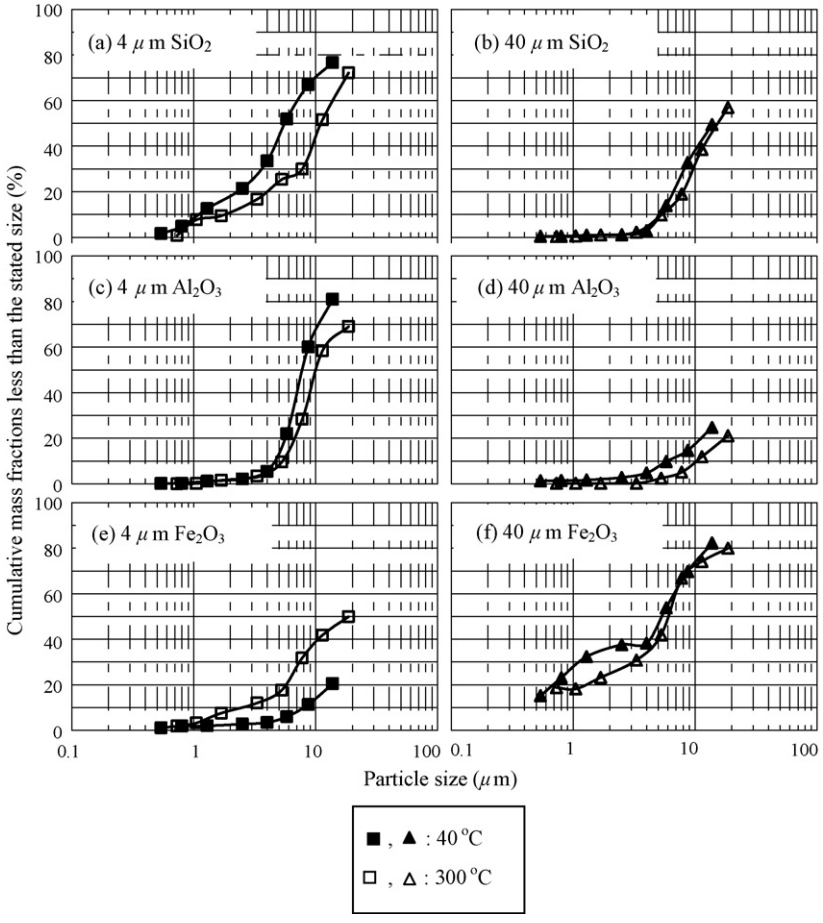

Fig. 6. Particle size distribution of the filtered SiO_2, Al_2O_3 and Fe_2O_3 particles in the exhaust gas at 40 and 300 °C.

Table 2a
SiO_2, Al_2O_3 and Fe_2O_3 compositions of the particles of different sizes when Al_2O_3 particles were filtered.

Particle size	4 μm Al_2O_3 was filtered			40 μm Al_2O_3 was filtered		
(μm)	SiO_2 (mg)	Al_2O_3 (mg)	Fe_2O_3 (mg)	SiO_2 (mg)	Al_2O_3 (mg)	Fe_2O_3 (mg)
>16.3	1.89	5.05	0.20	2.34	19.98	0.22
16.3	1.03	2.16	0.06	2.91	11.71	0.09
10.0	2.55	1.63	0.16	1.27	10.05	0.08
6.8	3.41	1.92	0.18	1.62	12.64	0.09
4.6	1.96	1.68	0.12	1.59	12.19	0.09
2.9	0.51	1.97	0.18	1.04	4.65	0.12
1.5	0.51	2.06	0.40	0.36	4.11	0.06
0.92	0.38	2.23	0.17	0.51	2.88	0.00
0.64	0.01	2.13	0.04	0.00	1.06	0.08

Table 2b
SiO_2, Al_2O_3 and Fe_2O_3 compositions of the particles of different sizes when Fe_2O_3 particles were filtered.

Particle size	4 μm Fe_2O_3 was filtered			40 μm Fe_2O_3 was filtered		
(μm)	SiO_2 (mg)	Al_2O_3 (mg)	Fe_2O_3 (mg)	SiO_2 (mg)	Al_2O_3 (mg)	Fe_2O_3 (mg)
>16.3	2.63	3.17	7.25	0.56	2.53	2.45
16.3	1.83	3.83	1.79	0.39	3.69	1.16
10.0	1.46	3.99	2.14	0.60	1.40	1.13
6.8	0.47	2.29	1.66	0.35	0.41	1.07
4.6	1.03	1.84	1.26	0.50	0.35	0.80
2.9	0.68	0.39	0.79	0.27	0.90	0.32
1.5	0.30	0.91	1.03	0.45	0.73	0.67
0.92	0.05	1.53	0.45	0.00	1.20	0.21
0.64	0.65	0.06	0.17	0.12	0.64	0.09

4.5. Chemical composition distributions of particles in the exit of a fluidized bed

Table 2 lists the Si, Al and Fe composition distributions of the variously sized particles in the exhaust gas associated with the filtering of Al_2O_3 and Fe_2O_3 particles. Si, Al and Fe were assumed to be present in the form of SiO_2, Al_2O_3 and Fe_2O_3. Since silica sand is mainly SiO_2, determining whether the Si content came from the silica sand or the filtered SiO_2 particles is difficult. Hence, the compositions were not analyzed when the SiO_2 particles were filtered. Table 2a lists the compositions of the filtered Al_2O_3 particles. The SiO_2 content was from the elutriated silica sand and the Fe_2O_3 content corresponded to the background concentration because only Al_2O_3 particles were added. The SiO_2 content of the large particles exceeded that of the small particles. The SiO_2 content of particles smaller than 2.9 μm was apparently lower than that of the large particles. Rodríguez et al. [31] explains that the small particles are not the most easily elutriated ones because they coagulate with each other or stick to large particles. The Fe_2O_3 content of the variously sized particles was equal and lower than that of the SiO_2 and Al_2O_3 since there were no Fe_2O_3 particles added. When the 4 μm Al_2O_3 particles were filtered, the Al_2O_3 content of the particles that was higher than 16.3 μm exceeded that of the small particles. The Al_2O_3 content of the particles that was smaller than 16.3 μm was constant with the variously sized particles. When the 40 μm Al_2O_3 particles were filtered, the Al_2O_3 content exceeded that of the 4 μm Al_2O_3 particles. As stated above, the collection efficiency of the 40 μm Al_2O_3 particles was much lower than that of the 4 μm Al_2O_3 particles. Therefore, the Al_2O_3 content in the filtered 40 μm Al_2O_3 particles was large. Moreover, the Al_2O_3 content declined as the particle size decreased.

Table 2b presents the composition of the filtered Al_2O_3 particles. The variation of SiO_2 content when the 4 μm Fe_2O_3 particles were filtered was similar to that of the Al_2O_3 particles. However, the SiO_2 content in the filtered 40 μm Fe_2O_3 particles was very low. Since the collection efficiency of the 40 μm Fe_2O_3 particles was high, the elutriated silica sand coagulated with the Fe_2O_3 particles and was captured in the bed. The Al_2O_3 content of the differently sized particles was almost independent of size when either the 4 or 40 μm Fe_2O_3 particles were filtered. The Fe_2O_3 content of the particles larger than 16.3 μm exceeded that of the small particles when the 4 and 40 μm Fe_2O_3 particles were filtered. The Fe_2O_3 content, when the 4 μm Fe_2O_3 particle was filtered, exceeded that of the 40 μm Fe_2O_3 particles indicating that the collection efficiency of the 40 μm Fe_2O_3 particles exceeded that of the 4 μm Fe_2O_3 particles.

4.6. Interparticle forces between filtered particles and bed material

In this work, the filtered particles were SiO_2, Al_2O_3 and Fe_2O_3. The difference in densities of the SiO_2, Al_2O_3 and Fe_2O_3 affected the gravity force on each. However, the van der Waal's force and electrostatic force were identical for them. Therefore, only the interparticle forces between the SiO_2 particles and the bed material were calcu-

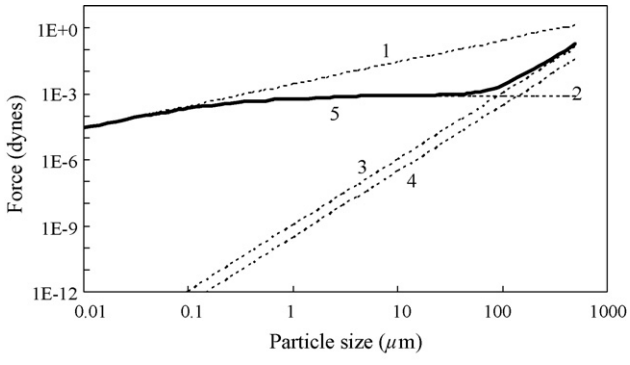

Fig. 7. Interparticle forces between the filtered particles and the bed material.

Table 3
The parameters used to calculate the interparticle forces.

ρ_p (kg/m^3)	A (J)	a (m)	RMS (m)	$\bar{\varepsilon}$	D_b (m)	ρ_b (kg/m^3)	E_d (V/m)	ε_0 (F/m)
2.3E+3	6.5E−20	3.0E−10	1.0E−7	0.43	0.155	1.3E+3	3.0E+6	8.85E−12

Table 4
The reciprocal equations used in the simulation process.

Interception[a] $E_R = \left(\frac{3}{\bar{\varepsilon}}\right)\overline{R}$, $\overline{R} = \frac{d_p}{d_c}$
Impaction[b] $E_I = 0.0583 \times Re_f \times S_t$, $S_t = \frac{\rho_p U_f d_p^2}{9\mu d_c} C_c$
Gravity[a] $E_G = G_a S_t$, $G_a = \frac{d_c g}{2U_f^2}$
Diffusion[a] $E_D = \frac{4.52}{(\bar{\varepsilon} P_e)^{1/2}}$, $P_e = \frac{d_c U_f}{D_p}$, $D_p = \frac{kT}{3\pi\mu d_p} C_c$,
$C_c = 1 + \frac{2\lambda}{d_p}\left[1.257 + 0.4\exp\left(-0.55\frac{d_p}{\lambda}\right)\right]$

[a] Tardos [18].
[b] Doganoglu [16].

lated in this work. Fig. 7 plots the gravity force, the van der Waal's force, the electrostatic force and the total force versus the diameter of the SiO_2 particles. Table 3 lists the parameters used to calculate the interparticle forces. The van der Waal's forces, calculated using the Hamaker or the R–R model, increased with the particle size and were approximately equal with particles smaller than 0.1 μm. For particles larger than 0.1 μm, the van der Waal's force increased with the particle size using the Hamaker model, but the increase in the van der Waal's force was lower according to the R–R model. The van der Waal's force was constant among particles that were larger than 1 μm according to the R–R model. The effect of asperity on the van der Waal's force diminished slowly as the particle size decreased. The gravity and electrostatic forces increased with the particle size with the same gradient. However, the magnitude of the gravity force always exceeded the electrostatic force by about an order of magnitude. The van der Waal's force and gravity force intersected at 70 μm. The gravity force overcame other forces when the particles were larger than 70 μm. In this study, most of the filtered particles were less than 40 μm, and therefore the van der Waal's force dominated.

4.7. Collection mechanisms and bounce-off effect

In earlier studies, some equations have been adopted to simulate the filtration efficiency of the various collection mechanisms. Table 4 lists the equations and parameters that were used. Fig. 8 shows the contribution of the individual mechanism to particle filtration. The gravity force on particles that were smaller than 100 μm was ignored. In this study, the fluidized bed filter was

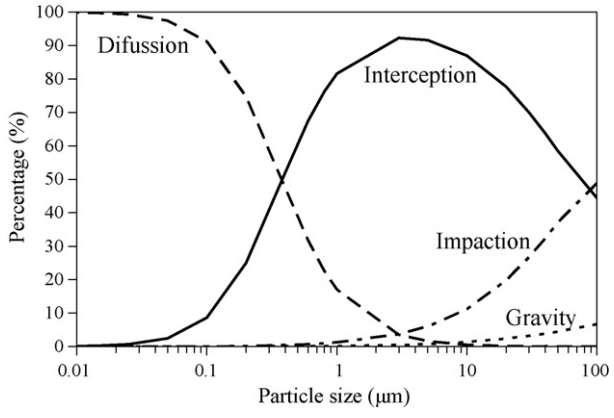

Fig. 8. Factions of the efficiency of individual mechanism on that of total mechanisms.

Table 5
The simulated single sphere collection efficiency.

d_p (μm)	E_T (%)	γ	E' (%)	d_p (μm)	E_T (%)	γ	E' (%)
270.0	99.9	1.75E−05	1.75E−03	7.0	7.0	1.57E−01	1.09E+00
193.6	99.9	4.01E−05	4.00E−03	5.0	4.9	3.55E−01	1.75E+00
138.8	99.9	9.19E−05	9.18E−03	3.2	3.1	1.00E+00	3.13E+00
99.5	99.9	2.11E−04	2.10E−02	2.3	2.3	1.00E+00	2.27E+00
71.4	86.8	4.83E−04	4.19E−02	1.6	1.7	1.00E+00	1.67E+00
51.2	64.2	1.11E−03	7.10E−02	1.2	1.3	1.00E+00	1.26E+00
36.7	44.9	2.53E−03	1.14E−01	0.85	1.0	1.00E+00	9.84E−01
26.3	30.7	5.80E−03	1.78E−01	0.61	0.8	1.00E+00	8.09E−01
18.9	21.0	1.33E−02	2.78E−01	0.44	0.7	1.00E+00	7.10E−01
13.5	14.4	3.03E−02	4.36E−01	0.35	0.7	1.00E+00	6.81E−01
9.7	10.0	6.90E−02	6.88E−01	0.31	0.7	1.00E+00	6.76E−01

E': the modified collection efficiency when the bounce-off effect is considered $E' = E_T \times \gamma$.

earthed and no external electrical field was added. Therefore, the electrostatic force in the bed was the weak Coulombic electrostatic force and weaker than the other dominating forces, as shown in Fig. 7. The effect of the electrostatic mechanism was regarded as negligible when no external electrical field existed [18]. The diffusion mechanism dominated for particles that were smaller than 0.4 μm. The removal efficiency of particles that were larger than 0.4 μm was governed mostly by the interception mechanism. However, the effect of the interception was the strongest for particles with a size of 4 μm and decreased sharply as the particle size increased. The effect of the impaction mechanism strengthened markedly with the particle size over 1 μm, weakening the effect of interception for large particles. In this study, the 4 and 40 μm particles were filtered. The interception mechanism was related mainly to the removal of particles of these sizes. However, the influence of impaction on removal efficiency was noticed for particles of size 40 μm.

All of the individual collection mechanisms worked to collect particles in a fluidized bed filter. Therefore, the total single sphere collection efficiency (E_T) was as given by Tardos [18].

$$E_T = 1 - [(1 - E_R)(1 - E_D)(1 - E_G)(1 - E_I)] \quad (7)$$

E_T must be corrected by multiplying it by the adhesion probability γ when the bounce-off effect is taken into consideration. Table 5 presents the simulated single sphere removal efficiency of the fly ash. The γ value increased rapidly as the particle size decreased, approaching unity when the particle size was larger than 3.2 μm. The E_T of particles that were larger than 100 μm exceeded 99% when the bounce-off effect was ignored. E_T fell as the particle size decreased to below 100 μm. When the bounce-off effect was taken into consideration, the collection efficiency of large particles declined significantly. The modified single sphere collection efficiency (E') increased from 1.75×10^{-3}% for a particle of size 270 μm to a maximum of 3.13% for a particle of size 3.2 μm, and then fell as the particle size decreased further. The effect of bounce off on the collection efficiency was negligible for particles that were smaller than 3.2 μm.

5. Conclusion

This work investigated the effect of interparticle forces and the collection mechanisms in particle filtration using a fluidized bed filter. SiO_2, Al_2O_3 and Fe_2O_3 particles with average sizes of 4 and 40 μm were filtered at 40 and 300 °C. When the 40 μm SiO_2 and

Al_2O_3 particles were filtered, the collection efficiency was zero at 40 and 300 °C. The bounce-off effect apparently reduced the collection efficiency although the strong impaction between 40 μm particles and bed material promoted the collisions between particles. The removal efficiency of the 4 μm SiO_2 and Al_2O_3 particles was 85–89% and 40–60% at 40 °C, 83–99% and 76–99% at 300 °C. The filtration of the Fe_2O_3 particles was inconsistent with the SiO_2 and Al_2O_3 particles. The removal efficiencies of the 40 μm Fe_2O_3 particles was 94–99%, exceeding that, 65–98%, of 4 μm Fe_2O_3 particles. The microstructures of SiO_2, Al_2O_3 and Fe_2O_3 particles indicated that the SiO_2 and Al_2O_3 particles were separate particles but that the Fe_2O_3 particles were formed by the agglomeration of very small particles. Strong impaction increased the collision between the Fe_2O_3 particles and the bed material and then strong interparticle forces promoted their mutual adherence, increasing the removal efficiency of the 40 μm Fe_2O_3 particles. The bounce-off effect weakened when strong interparticle forces were present.

As the particles entered the fluidized bed, abrasion between the particles and bed materials occurred. The hardness of the particles affected the abrasion of various particles. The hardness of the filtered particles and bed material followed the order $Al_2O_3 > SiO_2 \approx$ silica sand > Fe_2O_3. The Al_2O_3 particles were lightly abraded when they came into contact with silica sand. Hence, the sizes of the Al_2O_3 particles in the exit were close to the sizes of the input particles. In contrast, the Fe_2O_3 particles were heavily abraded so many small particles escaped from the fluidized bed filter.

Regarding the interparticle forces discussed herein, the van der waal's force dominated in particles that were smaller than 70 μm. The gravity force increased sharply with the particle size, exceeding the van der waal's force when the particles were larger than 70 μm. The diffusion mechanism dominated for particles that were smaller than 0.4 μm and the interception mechanism dominated for particles that were larger than 0.4 μm. Additionally, the effect of inertial impaction increased rapidly with the size of the particles above 1 μm. When large particles were filtered, strong impaction increased the collision between the filtered particles and the bed materials. However, the bounce-off effect suppressed the retention of particles by the bed material, affecting the collection efficiency. The bounce-off effect was diminished when a strong interparticle force was present between such particles as the Fe_2O_3 particles. The small particles approached the bed material by diffusion and were attached to the bed material by the van der waal's force. The bounce-off effect was negligible for small particles. A high collection efficiency of the very small particles was expected because of the strong diffusion mechanism and the weak bounce-off effect.

References

[1] P. Knettig, J.M. Beeckmans, Can. J. Chem. Eng. 52 (1974) 703–706.
[2] Y. Doganoglu, V. Jog, K.V. Thambimuthu, R. Clift, Removal of fine particles from gases in fluidized beds, Trans. IChemE. 56 (1978) 239–248.
[3] G. Tardos, N. Abuaf, C. Gutfinge, Atmos Environ. 10 (1976) 389–394.
[4] M.H. Peters, L.S. Fan, T.L. Sweeny, AIChE J. 28 (1982) 39–49.
[5] K. Ushiki, C. Tien, AIChE J. 30 (1984) 156–168.
[6] K. Ushiki, C. Tien, AIChE J. 32 (1986) 1606–1611.
[7] J. Baeyens, D. Geldart, S.Y. Wu, Powder Technol. 71 (1992) 71–80.
[8] S.E. George, J.R. Grace, Can. J. Chem. Eng. 59 (1981) 279–284.
[9] K. Smolders, J. Baeyens, Powder Technol. 92 (1997) 35–46.
[10] T. Baron, C.L. Briens, J.D. Hazlett, M.A. Bergougnou, P. Galtier, Can. J. Chem. Eng. 70 (1992) 631–635.
[11] M. Ghadiri, J.P.K. Seville, R. Clift, Trans. IChemE. 71 (1993) 371–381.
[12] C.A.P. Zevenhoven, Ph.D. thesis, Delft University of Technology. Delft, Netherlands, 1992.
[13] J.P.K. Seville, R. Clift, Blackie Academic & Professional, London, 1997.
[14] B.C. Chiang, M.Y. Wey, W.Y. Yang, J. Environ. Eng. 126 (2000) 985–992.
[15] B.C. Chiang, M.Y. Wey, C.L. Yeh, J. Hazard. Mater. 101 (B) (2003) 259–272.
[16] Y. Doganoglu, Ph.D. Dissertation, McGill Univ., Montreal, Canada, 1975.
[17] E.W. Schmidt, J.A. Gieseke, P. Gelfand, T.W. Lugar, D.A. Furlong, J. APCA. 28 (1978) 143–146.
[18] G.I. Tardos, in: M.E. Fayed, L. Otten (Eds.), Handbook of Powder Science & Technology, 2nd ed., Chapman and Hall, New York, NY, 1997.
[19] J.R. Coury, K.V. Thambimuthu, R. Clift, Powder Technol. 50 (1987) 253–265.
[20] C. Tien, Granular Filtration of Aerosols and Hydrosols, Butterworths, London, 1989.
[21] Y.I. Rabinovich, J.J. Adler, M.S. Esayanur, A. Ata, R.K. Singh, B.M. Moudgil, Adv. Colloid Interface Sci. 96 (2002) 213–230.
[22] M.C. Coelho, N. Harnby, Powder Technol. 20 (1978) 197–200.
[23] H.C. Hamaker, Physica 4 (1937) 1058–1072.
[24] K.L. Johnson, K. Kendall, A.D. Roberts, Proceedings of the Royal Society of London, A 324 (1971) 301–313.
[25] B.V. Derjaguin, V.M. Muller, Y.P. Toporov, Colloid Interface Sci. 53 (1975) 314–326.
[26] H. Rumpf, Particle Technology, Chapman and Hall, London, 1990.
[27] Y.I. Rabinovich, J.J. Adler, A. Ata, R.K. Singh, B.M. Moudgil, J. Colloid Interface Sci. 232 (2000) 10–16.
[28] J. Revel, C. Gatumel, J.A. Dodds, J. Taillet, Powder Technol. 135–136 (2003) 192–200.
[29] K.Y. Liu, M.Y. Wey, Fuel 86 (2007) 161–168.
[30] M.Y. Wey, K.H. Chen, K.Y. Liu, J. Hazard. Mater. 121 (B) (2005) 175–181.
[31] J.M. Rodr-guez, J.R. S-nchez, A. Alvaro, D.F. Florea, A.M. Est-vez, Powder Technol. 11 (2000) 218–230.